Hindawi
International Journal of Photoenergy
Volume 2018, Article ID 8516356, 6 pages
https://doi.org/10.1155/2018/8516356

Research Article

Preparation and Physical and Photocatalytic Activity of a New Niobate Oxide Material Containing NbO_4 Tetrahedra

Hengkai Pan,[1,2] Bei Wang,[1,2] Feng Zhang,[1,2] Weifeng Zhang,[1,2] and Guoqiang Li[1,2]

[1]*Henan Key Laboratory of Photovoltaic Materials, Henan University, Kaifeng 475004, China*
[2]*Laboratory of Low-Dimensional Materials Science, Henan University, Kaifeng 475004, China*

Correspondence should be addressed to Feng Zhang; zhangfeng.home@163.com and Guoqiang Li; gqli1980@henu.edu.cn

Received 2 April 2018; Revised 19 July 2018; Accepted 9 August 2018; Published 4 September 2018

Academic Editor: Leonardo Palmisano

Copyright © 2018 Hengkai Pan et al. This is an open access article distributed under the Creative Commons Attribution License, which permits unrestricted use, distribution, and reproduction in any medium, provided the original work is properly cited.

The shape and connection type of MO_x are critical to the physical and chemical properties. A series of new material $Sr_{2-x}Na_xNbO_4$ containing NbO_4 tetrahedra was prepared by controlling the ratio of $SrCO_3$ to sodium niobate under ambient air. With increasing the content of Sr in the sample, the MO_x shape will change from NbO_6 octahedra to NbO_4 tetrahedra, which is confirmed by the Raman scattering spectra. With increasing the content of NbO_4 in the sample, the lattice parameter increases, optical band gap becomes larger, and the surface changes to be more active for oxygen adsorption, resulting in a higher photocatalytic activity.

1. Introduction

Complex metal oxide (AMO_y) is built upon the framework of MO_x with sharing edges or corners and the inserted metal ion. The shape of MO_x is diverse, such as octahedron and tetrahedron. The shape and connection types of MO_x are critical to the physical and chemical properties [1–5]. Recently, theoretical predictions and experimental results confirmed that the TaS_2 built from the edge-sharing of TaS_6 trigonal prisms exhibits superior catalytic performance in comparison with that of TaS_6 octahedra [6, 7]. Those early studies suggested a potential way to improve the catalytic activity via tuning the shape of MO_x. The above hypothesis is rarely investigated in niobates, which is one kind of photocatalyst for water splitting and organic degradation, such as $NaNbO_3$, $SrNb_2O_6$, and $Cs_2Nb_4O_{11}$ [8–15]. Most of the niobate photocatalysts contain NbO_6 octahedra. For instance, $NaNbO_3$ contains the formwork of NbO_6 octahedra sharing corners with a slight distortion [16, 17]. The NbO_6 octahedra in $SrNb_2O_6$ share edges and corners simultaneously [14]. $Cs_2Nb_4O_{11}$ is the one that coexisted with NbO_6 octahedra and NbO_4 tetrahedra in the structure [12, 18]. The tetrahedral NbO_4 structure is rarely found in niobium oxide compounds because the Nb^{5+} atom is usually too large to fit into an oxygen-anion tetrahedron and exists in the rare earth $ANbO_4$ (A = Y, Sm, and La) compounds [1, 2, 19]. To investigate the effect of MO_x shape on photocatalytic activity, the challenge is preparing the sample containing NbO_4 tetrahedra.

Here, we reported a series of new material $Sr_{2-x}Na_xNbO_4$ containing NbO_4 tetrahedra, which was prepared from sodium niobate and $SrCO_3$ with different ratios under ambient air. The MO_x shape will change from NbO_6 octahedra to NbO_4 tetrahedra. The Raman results identified that NbO_4 tetrahedra existed in the samples. The change from the NbO_6 octahedra to NbO_4 tetrahedra results in the different physical and chemical properties, such as optical band gap, adsorption property, and photocatalytic activity.

2. Experimental Section

2.1. Sample Preparation. Sodium niobate precursor was synthesized via a simple hydrothermal process. Typically, the prepared mixture of 50 mL of NaOH solution (8 M) and 2 g of Nb_2O_5 powder was poured into a 100 mL teflon-lined stainless steel autoclave. The hydrothermal reaction was performed in a drying oven at 120°C for 3 h [20–22]. After

naturally cooling down to room temperature, we obtained the samples and rinsed the samples with deionized water and absolute ethanol to remove the residual unreacted precursor. The sodium niobate precursor was confirmed as the $Na_2Nb_2O_6 \bullet xH_2O$ from the XRD.

$SrCO_3$ and sodium niobate precursor were mixed in the mortar at different molar ratios and grounded for 15 min. Then, they were heated at 500°C for 3 h and calcined at 800°C for 10 h in a muffle furnace. After cooling, we got the samples. For simplicity, we denoted the samples prepared from the ratios of $SrCO_3$ to sodium niobate precursor of 1 : 2, 2 : 2, and 4 : 2 as A, B, and C, respectively. For comparison, the sample was also prepared by solid state reaction method using $NaNbO_3$ and $SrCO_3$ as starting materials at 900°C for 10 h.

2.2. Characterizations. The crystal structures were identified by X-ray diffraction (XRD). Raman scattering spectrum was measured using a laser Raman spectrophotometer at room temperature. The X-ray photoelectron spectra (XPS) were measured by a Kratos AXIS Ultra photoelectron spectroscope. The diffusion reflection spectrum was recorded with a UV-vis spectrophotometer (Shimadzu 2550) using $BaSO_4$ as the reference and transformed to the absorption spectra automatically. The temperature programmed desorption (TPD) was carried out on Chembet Pulsar TPD using He pretreatment at 300°C for 1 h. Inductively coupled plasma (ICP) was performed on Agilent 720/730 after pretreatment in mixture of HCl and HNO_3.

Photocatalytic activity for the decomposition of RhB in an aqueous solution was evaluated in the presence of samples A, B, and C under full arc light irradiation of Xe lamp as reported previously [23]. The initial concentration and pH value of RhB solution were about 2.5 mg L^{-1} and 4.5. Before illumination, the reagent was left in the dark for 30 min to achieve adsorption-desorption equilibrium. After adsorption of dye, the pH value is 6.7 for sample A, 6.6 for sample B, and 8.5 for sample C. The light emitted from the 300-W Xe lamp (the spectra is the same as that in our previous report [24]) directly irradiated on the solution in the reactor. The stirring was on during the reaction. The variation in the concentration of RhB was recorded by measuring the absorbance of the main peak in the UV-vis spectrum (UV-2550, Shimadzu) every 30 min.

3. Results and Discussions

All the samples show the similar XRD patterns with that of Sr_2NbO_4 (PDF#28-1245), as shown in Figure 1(a) [25]. A slight amount of $SrCO_3$ impurity was found in sample C due to too much $SrCO_3$ in the starting mixture. The compositions of samples were determined as $Sr_{0.6}Na_{1.4}NbO_4$, $Sr_{0.97}Na_{1.03}NbO_4$, and $Sr_{1.73}Na_{0.27}NbO_4$ for A, B, and C, from the ICP results. The total charge at A site will increase from 2.8 for sample A, 2.97 for sample B, and up to 3.73 for sample C. Moreover, the positions of diffraction peaks were successively shifted towards smaller 2θ with increasing the content of $SrCO_3$, as shown in Figure 1(b). Two factors, namely strains and lattice parameter changes, will contribute to the shift of diffraction peaks [26]. The strains could be estimated by the following equations.

$$\frac{\beta \cos\theta}{\lambda} = \frac{1}{D} + \frac{\eta \sin\theta}{\lambda}, \quad (1)$$

where β is the full width at half-maximum (FWHM) of the θ-2θ peak; θ is the diffraction angle; λ is the X-ray wavelength; η is the effective strain, and D is the crystallite size. The strain (η) is calculated from the slope, and the crystallite size (D) is calculated from the intercept of a plot of $\beta \cos \theta/\lambda$ against $\sin \theta/\lambda$. The calculated effective strain of samples A, B, and C are 1.15%, 0.87%, and 0.41%, respectively. However, the decrease in the effective strain is not reasonable. Kumar et al. found that the diffraction peak of $NaNbO_3$/CdS core/shell particles shifted to larger 2θ in comparison with pristine $NaNbO_3$, where the effective strain of $NaNbO_3$/CdS core/shell particles will decrease down to −0.76% from 0.89% for $NaNbO_3$ [26]. Our result is opposite to the above tendency, so we thought the shift of diffraction peak is not caused by the strains. According to the Bragg's law, we calculated the lattice parameter using Sr_2NbO_4 as the parent structure, as shown in Figure 1(c). It is clearly seen that the lattice parameter increases with the rise in the content of Sr and trend towards 4.11 Å that of Sr_2NbO_4.

Raman scattering is an effective method of investigating the changes at local structure. Figure 2(a) shows Raman scattering spectra of samples prepared from different ratios. The Raman band near 780–840 cm^{-1} appears in all the samples, whereas the band near 500–600 cm^{-1} only existed in sample A. The Raman band around 780–830 cm^{-1} is corresponding to the vibrational modes of a regular NbO_4 tetrahedron, and the band near 500–700 cm^{-1} is assigned as the symmetric stretching mode of the NbO_6 octahedra [1, 18, 19]. The correlation between the Raman wavenumbers for the stretching bands in niobate compounds and the Nb-O bond length has previously been established. We calculated the Nb-O bond length using the empirical equation $\nu/cm^{-1} = 29522 \times \exp(-1.9168R)$, where ν is the Nb-O stretching wavenumber, and R is the Nb-O bond length [13, 27]. The results are shown in Figure 2(b), and all of the Nb-O length satisfied the requirement of Nb-O bond length in NbO_4 tetrahedron of 1.83–1.93 Å, indicating that all the samples contain NbO_4 tetrahedron [1]. The precursor of sodium niobate only has the band near 500–600 cm^{-1}, and the $YNbO_4$ contains the Raman band near 780-840 cm^{-1}. Above results confirmed that sample A contains NbO_6 octahedran and NbO_4 tetrahedra, and samples B and C mainly contain NbO_4 tetrahedron. The formation mechanism will be discussed later. The Nb-O bond length increases with the rise in the content of Sr.

The optical properties of samples are displayed in Figure 3. The absorption edge of sample A locates at ~324 nm corresponding to ~3.8 eV, whereas that of samples B and C is ~310 nm corresponding to ~4.0 eV, implying that sample A has a narrower band gap in comparison with samples B and C. The increase of lattice distance usually results in the larger band gap due to the smaller expansion of the energy levels according to the principle of solid state physics.

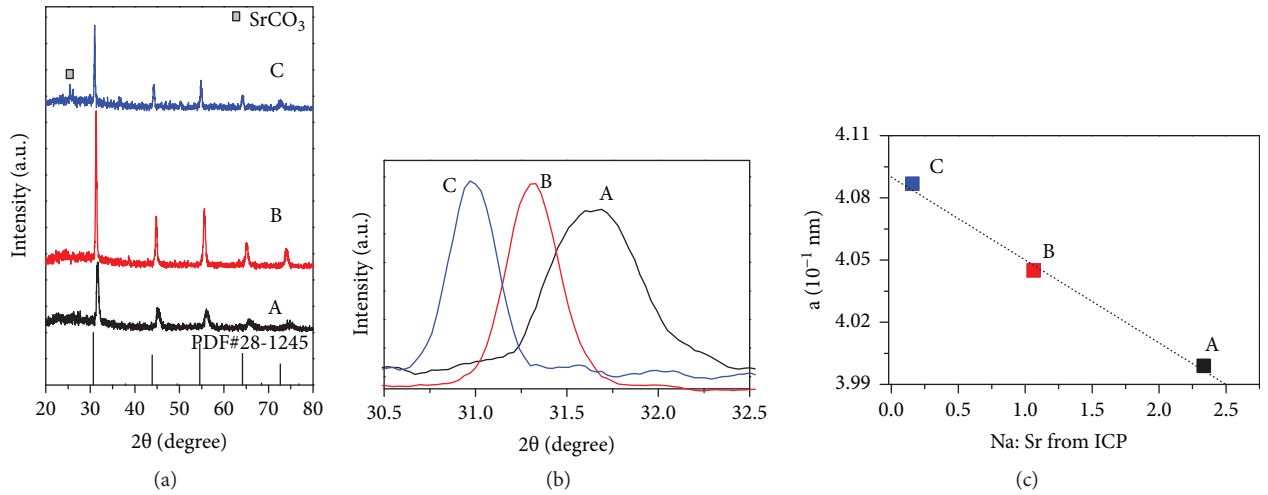

Figure 1: (a) XRD patterns, (b) enlarged view of main peak, (c) lattice parameter vs. Na : Sr ratio of samples prepared from different ratio of $SrCO_3$ to sodium niobate of (A) 1 : 2, (B) 2 : 2, and (C) 4 : 2. The standard XRD pattern of Sr_2NbO_4 (PDF#28-1245) was plotted at the bottom in Figure 1(a).

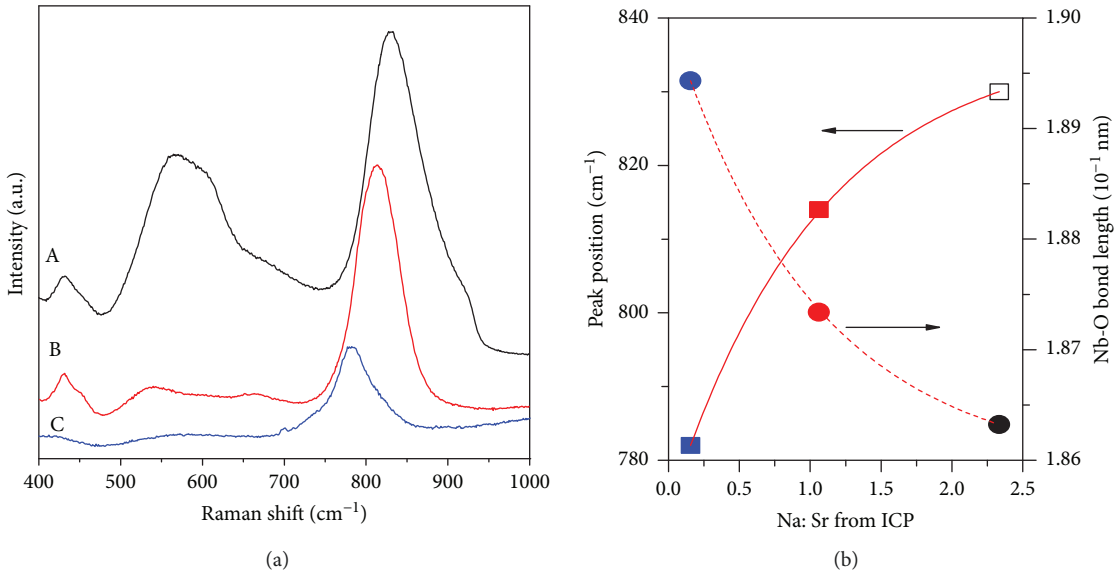

Figure 2: (a) Raman scattering spectra of samples prepared from different ratios and (b) plot of Raman peak position vs. Na : Sr ratio.

Consequently, it is reasonable to get the bigger optical band gap in samples B and C because they have larger lattice parameter. Samples B and C have the similar absorption edge and band gap, which is possibly attributed to their common properties of containing NbO_4 tetrahedra. Sample C has a tail around 310–500 nm, indicating that sample C possibly has more defects in comparison with sample B.

The O1s XPS lines obtained from samples are shown in Figure 4. The binding energies were calibrated to the C1s peak at 284.8 eV. The O1s spectra can be divided into two peaks at 530.0 and 531.4 eV, respectively. The peak at 530.0 eV represents the binding energy of lattice oxygen ions [28–31]. The peak at 531.4 eV was considered as the binding energy of oxygen defects [31] or surface oxygen, such as O_2^- [29, 30]. The ratio of O_{ads} to O_{latt} increases with the rise in the content of Sr. We used the TPD to investigate the property of

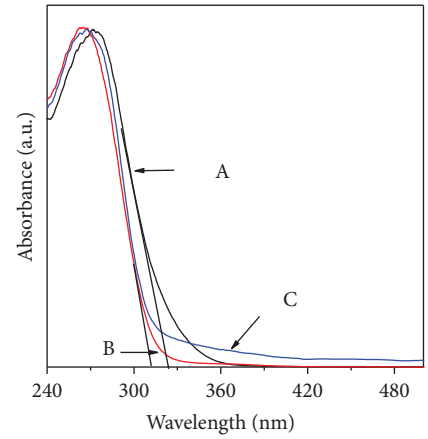

Figure 3: UV-vis spectra of samples prepared from different ratios.

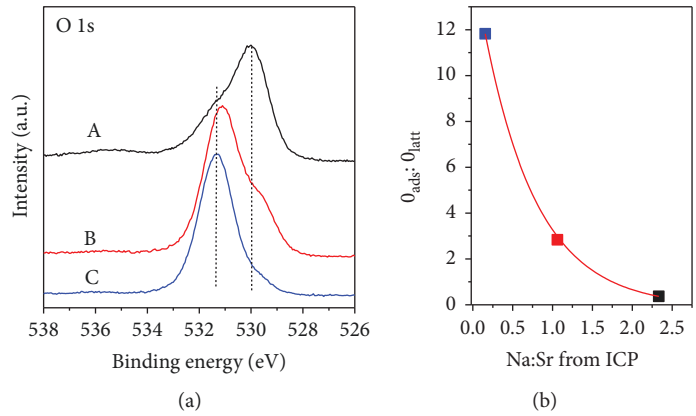

Figure 4: (a) O1s XPS lines obtained from samples and (b) the ratio of O_{ads} to O_{latt} change with Na : Sr ratio in the sample.

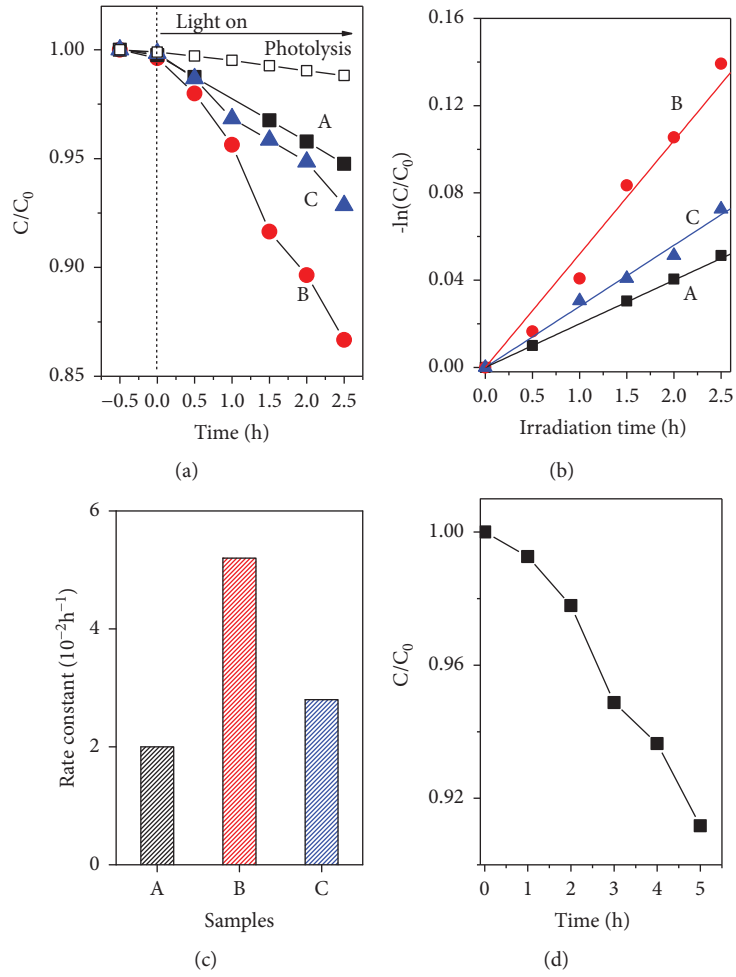

Figure 5: (a) RhB concentration varied with reaction time, (b) plot of $-\ln(C/C_0)$ vs. time, (c) the rate constant of all the samples, and (d) dichlorid phenol concentration varied with reaction time over sample B.

oxygen adsorption. The amount of adsorbed oxygen on samples is consistent with the XPS results.

Photocatalytic activity was evaluated by the photocatalytic RhB photodegradation under 300-W Xe lamp. Figure 5(a) shows the RhB concentration varied with reaction time. Obviously, after irradiation, the RhB concentration is decreased. When the reagent solution is dilute, the reaction rate (r) can be expressed as $r = kC$, where k is the apparent rate constant, and C is the instantaneous concentration of the reactant. The plots of $-\ln(C/C_0)$ vs. time are shown in Figure 5(b), and the rate constants of RhB degradation are also displayed in Figure 5(c). k is 2.0×10^{-2}, 5.2×10^{-2}, and

2.8×10^{-2} h^{-1} for samples A, B, and C, respectively. Sample B exhibits 2.6 times higher activity than sample A. Dichlorid phenol (DCP), a colorless toxic pollutant, was used as a model pollutant, as shown in Figure 5(d). The DCP concentration was decreased over the sample B.

We will address the formation mechanism of NbO_4 tetrahedra and how to affect the photocatalytic activity. Usually the Sr_2NbO_4 could be synthesized under vacuum or reduced atmosphere [25]. In this work, we used sodium niobate as one of the starting materials and got $Sr_{2-x}Na_xNbO_4$ under ambient air. When sodium niobate reacts with $SrCO_3$, the Sr^{2+} will substitute Na^+. The Sr atom will give one excess charge and create an equivalent reduced atmosphere, resulting in the change of NbO_6 octahedra to NbO_4 tetrahedra. With increasing the content of Sr in the structure, the lattice parameter will be increased due to larger ionic radius of Sr^{2+} (1.18 Å) than Na^+ (1.02 Å) [16]. More amount of Sr inserted into the structure will cause the unbalance charge in A site (AMOx), leading to more defects generated in the sample, as that observed in sample C. Moreover, we could get the Na-doped Sr_2NbO_4 via the solid state reaction method using pseudoperovskite $NaNbO_3$ as the starting material, indicating that Na is very important to get $Sr_{2-x}Na_xNbO_4$, not the structure of sodium niobate. With increasing the content of NbO_4 in the sample, supported by the results of Raman spectra, the lattice parameter increases, optical band gap becomes larger, and the surface changes to be more active for oxygen adsorption, resulting in a higher photocatalytic activity. Above trends could be obtained from the results of samples A and B, supporting the catalytic property of MO_4 tetrahedron is superior to that of MO_6 octahedron. Due to more defects in sample C, its photocatalytic activity decreases in comparison with sample B.

4. Conclusions

We prepared a series of $Sr_{2-x}Na_xNbO_4$ photocatalytic materials containing NbO_4 tetrahedra by controlling the ratio of $SrCO_3$ to sodium niobate under ambient air. With increasing the content of NbO_4 in the sample, the lattice parameter increases, optical band gap becomes larger, and the surface changes to be more active for oxygen adsorption, resulting in a higher photocatalytic activity. The efficiency of this catalyst can also be due to the photosensibilisation of RhB and should be tested by using another organic molecule as model pollutant.

Data Availability

The data used to support the findings of this study are available from the corresponding author upon request.

Conflicts of Interest

The authors declare that they have no conflicts of interest.

Acknowledgments

This work was supported by the Young Core Instructor Foundation from the Education Commission of Henan Province (2015GGJS-021), the Program for Science & Technology Innovation Talents in Universities of Henan Province, China (17HASTIT014), and Henan University funding (0000A40374).

References

[1] J. M. Jehng and I. Wachs, "Structural chemistry and Raman spectra of niobium oxides," *Chemistry of Materials*, vol. 3, no. 1, pp. 100–107, 1991.

[2] K. Nakajima, Y. Baba, R. Noma et al., "$Nb_2O_5 \cdot nH_2O$ as a heterogeneous catalyst with water-tolerant Lewis acid sites," *Journal of the American Chemical Society*, vol. 133, no. 12, pp. 4224–4227, 2011.

[3] M. M. Ahmad, E. S. Yousef, and E. S. Moustafa, "Dielectric properties of the ternary $TeO_2/Nb_2O_5/ZnO$ glasses," *Physica B: Condensed Matter*, vol. 371, no. 1, pp. 74–80, 2006.

[4] H. Chen, F. Zhang, W. Zhang, Y. Du, and G. Li, "Negative impact of surface Ti^{3+} defects on the photocatalytic hydrogen evolution activity of $SrTiO_3$," *Applied Physics Letters*, vol. 112, no. 1, article 013901, 2018.

[5] G. Q. Li, Z. G. Yi, H. T. Wang, C. H. Jia, and W. F. Zhang, "Factors impacted on anisotropic photocatalytic oxidization activity of ZnO: surface band bending, surface free energy and surface conductance," *Applied Catalysis B: Environmental*, vol. 158-159, pp. 280–285, 2014.

[6] D. N. Chirdon and Y. Wu, "Hydrogen evolution: not living on the edge," *Nature Energy*, vol. 2, no. 9, article 17132, 2017.

[7] Y. Liu, J. Wu, K. P. Hackenberg et al., "Self-optimizing, highly surface-active layered metal dichalcogenide catalysts for hydrogen evolution," *Nature Energy*, vol. 2, no. 9, article 17127, 2017.

[8] H. Wang, L. Zhang, Z. Chen et al., "Semiconductor heterojunction photocatalysts: design, construction, and photocatalytic performances," *Chemical Society Reviews*, vol. 43, no. 15, pp. 5234–5244, 2014.

[9] F. E. Osterloh, "Inorganic nanostructures for photoelectrochemical and photocatalytic water splitting," *Chemical Society Reviews*, vol. 42, no. 6, pp. 2294–2320, 2013.

[10] H. Shi, G. Chen, C. Zhang, and Z. Zou, "Polymeric g-C_3N_4 coupled with $NaNbO_3$ nanowires toward enhanced photocatalytic reduction of CO_2 into renewable fuel," *ACS Catalysis*, vol. 4, no. 10, pp. 3637–3643, 2014.

[11] Q. N. Yu, F. Zhang, G. Q. Li, and W. F. Zhang, "Preparation and photocatalytic activity of triangular pyramid $NaNbO_3$," *Applied Catalysis B: Environmental*, vol. 199, pp. 166–169, 2016.

[12] Y. Miseki, H. Kato, and A. Kudo, "Water splitting into H_2 and O_2 over $Cs_2Nb_4O_{11}$ photocatalyst," *Chemistry Letters*, vol. 34, no. 1, pp. 54-55, 2005.

[13] I.-S. Cho, S. Lee, J. H. Noh et al., "$SrNb_2O_6$ nanotubes with enhanced photocatalytic activity," *Journal of Materials Chemistry*, vol. 20, no. 19, article 3979, 2010.

[14] D. Chen and J. H. Ye, "Selective-synthesis of high-performance single-crystalline $Sr_2Nb_2O_7$ nanoribbon and $SrNb_2O_6$ nanorod photocatalysts," *Chemistry of Materials*, vol. 21, no. 11, pp. 2327–2333, 2009.

[15] Y. Miseki, H. Kato, and A. Kudo, "Water splitting into H_2 and O_2 over niobate and titanate photocatalysts with (111) plane-type layered perovskite structure," *Energy & Environmental Science*, vol. 2, no. 3, p. 306, 2009.

[16] G. Q. Li, T. Kako, D. F. Wang, Z. G. Zou, and J. Ye, "Composition dependence of the photophysical and photocatalytic properties of $(AgNbO3)_{1-x}(NaNbO3)_x$ solid solutions," *Journal of Solid State Chemistry*, vol. 180, no. 10, pp. 2845–2850, 2007.

[17] P. Li, S. X. Ouyang, G. C. Xi, T. Kako, and J. H. Ye, "The effects of crystal structure and electronic structure on photocatalytic H_2 evolution and CO_2 reduction over two phases of perovskite-structured $NaNbO_3$," *The Journal of Physical Chemistry C*, vol. 116, no. 14, pp. 7621–7628, 2012.

[18] J. Liu, E. P. Kharitonova, C. G. Duan, W. N. Mei, R. W. Smith, and J. R. Hardy, "Phase transition in single crystal $Cs_2Nb_4O_{11}$," *The Journal of Chemical Physics*, vol. 122, no. 14, article 144503, 2005.

[19] J. Pellicer-Porres, A. B. Garg, D. Vázquez-Socorro, D. Martínez-García, C. Popescu, and D. Errandonea, "Stability of the fergusonite phase in $GdNbO_4$ by high pressure XRD and Raman experiments," *Journal of Solid State Chemistry*, vol. 251, pp. 14–18, 2017.

[20] H. Zhu, Z. Zheng, X. Gao et al., "Structural evolution in a hydrothermal reaction between Nb_2O_5 and NaOH solution: - from Nb2O5 grains to microporous $Na_2Nb_2O_6{\cdot}2/3H_2O$ fibers and $NaNbO_3$ cubes," *Journal of the American Chemical Society*, vol. 128, no. 7, pp. 2373–2384, 2006.

[21] H. Xu, M. Nyman, T. M. Nenoff, and A. Navrotsky, "Prototype Sandia octahedral molecular sieve (SOMS) $Na_2Nb_2O_6{\cdot}H_2O$: - synthesis, structure and thermodynamic stability," *Chemistry of Materials*, vol. 16, no. 10, pp. 2034–2040, 2004.

[22] M. N. Iliev, M. L. F. Phillips, J. K. Meen, T. M. Nenoff, and J. Phys, "Raman spectroscopy of $Na_2Nb_2O_6{\bullet}H_2O$ and $Na_2Nb_{2-x}MxO_{6-x}(OH)_x{\bullet}H_2O$ (M = Ti, Hf) ion exchangers," *The Journal of Physical Chemistry B*, vol. 107, no. 51, pp. 14261–14264, 2003.

[23] G. Q. Li, N. Yang, W. L. Wang, and W. F. Zhang, "Synthesis, photophysical and photocatalytic properties of N-doped sodium niobate sensitized by carbon nitride," *Journal of Physical Chemistry C*, vol. 113, no. 33, pp. 14829–14833, 2009.

[24] W. L. Wang, G. Q. Li, N. Yang, and W. F. Zhang, "Composition dependence of surface photoelectric and photodegradation activities of silver antimonates with pyrochlore-like structure," *Materials Chemistry and Physics*, vol. 123, no. 1, pp. 322–325, 2010.

[25] K. Isawa and M. Nagano, "Synthesis and physical properties of niobium-based oxide, $Sr_{2-x}La_xNbO4$ ($0 \leqslant x < 0.2$)," *Physica C Superconductivity*, vol. 357–360, pp. 359–362, 2001.

[26] S. Kumar, S. Khanchandani, M. Thirumal, and A. K. Ganguli, "Achieving enhanced visible-light-driven photocatalysis using type-II $NaNbO_3$/CdS core/shell heterostructures," *ACS Applied Materials & Interfaces*, vol. 6, no. 15, pp. 13221–13233, 2014.

[27] F. D. Hardcastle and I. E. Wachs, "Determination of vanadium-oxygen bond distances and bond orders by Raman spectroscopy," *The Journal of Physical Chemistry*, vol. 95, no. 13, pp. 5031–5041, 1991.

[28] H. Tan, Z. Zhao, W. B. Zhu et al., "Oxygen vacancy enhanced photocatalytic activity of pervoskite $SrTiO_3$," *ACS Applied Materials & Interfaces*, vol. 6, no. 21, pp. 19184–19190, 2014.

[29] T. Kanagaraj and S. Thiripuranthagan, "Photocatalytic activities of novel $SrTiO_3$ – BiOBr heterojunction catalysts towards the degradation of reactive dyes," *Applied Catalysis B: Environmental*, vol. 207, pp. 218–232, 2017.

[30] K. Xie, N. Umezawa, N. Zhang, P. Reunchan, Y. Zhang, and J. Ye, "Self-doped $SrTiO_{3-\delta}$ photocatalyst with enhanced activity for artificial photosynthesis under visible light," *Energy & Environmental Science*, vol. 4, no. 10, article 4211, 2011.

[31] W. Yu, G. Ou, W. Si, L. Qi, and H. Wu, "Defective $SrTiO_3$ synthesized by arc-melting," *Chemical Communications*, vol. 51, no. 86, pp. 15685–15688, 2015.

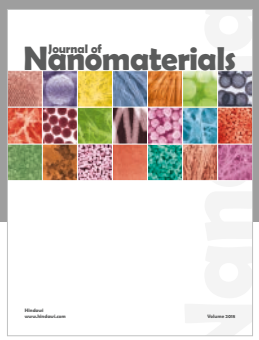

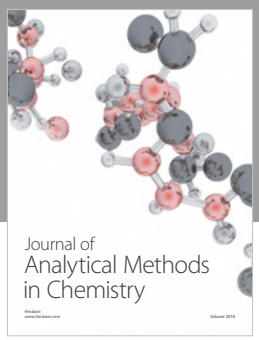

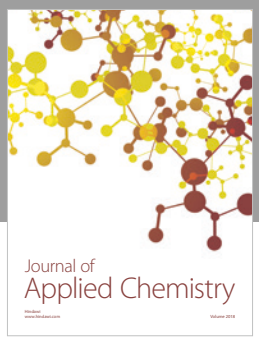

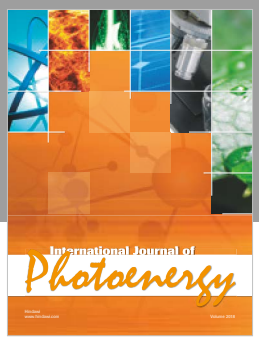

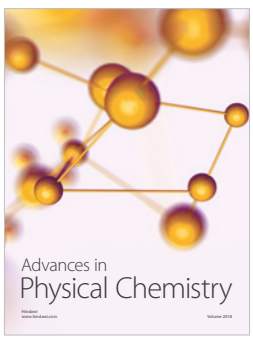

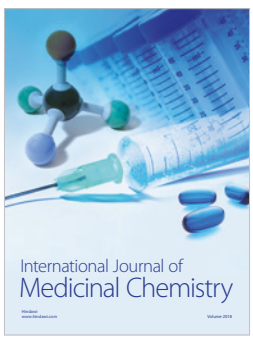

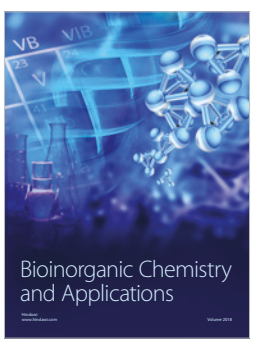

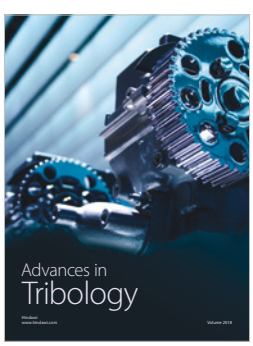

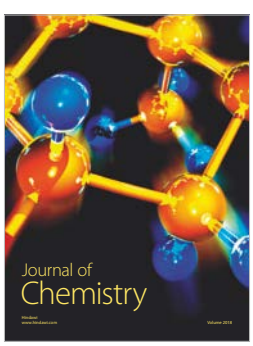

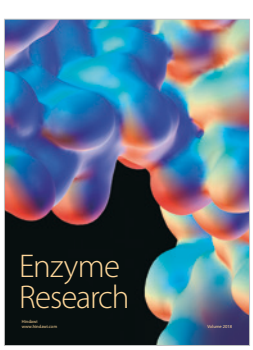

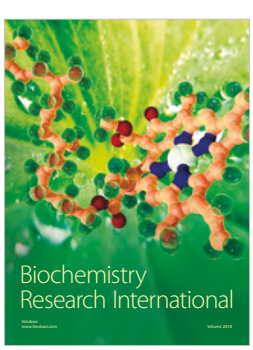

Hindawi

Submit your manuscripts at
www.hindawi.com